UNIVERSITYᴼF BIRMINGHAM

Research at Birmingham

Active release of pneumolysin prepores and pores by mammalian cells undergoing a Streptococcus pneumoniae attack

Wolfmeier, Heidi; Radecke, Julika; Schoenauer, Roman; Koeffel, René; Babiychuk, Viktoria S.; Drücker, Patrick; Hathaway, Lucy J.; Mitchell, Timothy; Zuber, Benoît; Draeger, Annette; Babiychuk, Eduard B.

Link to publication on Research at Birmingham portal

Accepted Manuscript

Active release of pneumolysin prepores and pores by mammalian cells undergoing a *Streptococcus pneumoniae* attack

Heidi Wolfmeier, Julika Radecke, Roman Schoenauer, René Koeffel, Viktoria S. Babiychuk, Patrick Drücker, Lucy J. Hathaway, Timothy J. Mitchell, Benoît Zuber, Annette Draeger, Eduard B. Babiychuk

Active release of pneumolysin prepores and pores by mammalian cells undergoing a *Streptococcus pneumoniae* attack.

Heidi Wolfmeier[a,*], Julika Radecke[a,b,*], Roman Schoenauer[a], René Koeffel[a], Viktoria S. Babiychuk[a], Patrick Drücker[a], Lucy J. Hathaway[c], Timothy J. Mitchell[d], Benoît Zuber[a,‡], Annette Draeger[a], Eduard B. Babiychuk[a,‡]

[a] Institute of Anatomy, University of Bern, Baltzerstrasse 2, 3000 Bern 9, Switzerland.

[b] Graduate School for Cellular and Biomedical Sciences, University of Bern, Freiestrasse 1, 3000 Bern 9, Switzerland.

[c] Institute for Infectious Diseases, University of Bern, Friedbühlstrasse 51, Postfach, 3001 Bern, Switzerland.

[d] Institute of Microbiology and Infection, College of Medical and Dental Sciences, University of Birmingham, Edgbaston, Birmingham, B15 2TT, United Kingdom.

[*] Joint first authorship

[‡] Corresponding authors: Institute of Anatomy, University of Bern, Baltzerstrasse 2, 3000 Bern 9, Switzerland

Tel.: +41 (0) 31 631 30 86, Fax: +41 (0) 31 631 38 07

E-mail: edik@ana.unibe.ch, benoit.zuber@ana.unibe.ch

Abbreviations: AEC, primary human airway epithelial cells; ALG-2, apoptosis-linked gene 2; ALIX, ALG-2 interacting protein X; BCA, bicinchoninic acid; CCD, charge-coupled device; CDC, cholesterol-dependent cytolysins; Chmp4B, charged multivesicular body protein 4B; ESCRT, endosomal sorting complex required for transport; FACS, fluorescence activated cell sorting; FBS, Fetal Bovine Serum; FT, Fourier transform detector; HBE, human bronchial epithelial cells; HEK 293, human embryonic kidney cells; HRP, horseradish peroxidase; Hsp90, heat shock protein 90; NAD, nonlinear anisotropic diffusion; PBS, phosphate buffered saline; PLY, pneumolysin; PMSS, protein match score summation; PVDF, polyvinylidene difluoride; SDS-PAGE, sodium dodecyl sulfate polyacrylamide gel electrophoresis; SLO, streptolysin O; Vps4, vacuolar protein sorting 4.

Abstract

BACKGROUND. *Streptococcus pneumoniae* is a potent human pathogen. Its pore-forming exotoxin pneumolysin is instrumental for breaching the host's epithelial barrier and for the incapacitation of the immune system.

METHODS and RESULTS. Using a combination of life imaging and cryo-electron microscopy we show that pneumolysin, released by cultured bacteria, is capable of permeabilizing the plasmalemma of host cells. However, such permeabilization does not lead to cell lysis since pneumolysin is actively removed by the host cells. The process of pore elimination starts with the formation of pore-bearing plasmalemmal nanotubes and proceeds by the shedding of pores that are embedded in the membrane of released microvesicles. Pneumolysin prepores are likewise removed. The protein composition of the toxin-induced microvesicles, assessed by mass spectrometry, is suggestive of a Ca^{2+}-triggered mechanism encompassing the proteins of the annexin family and members of the endosomal sorting complex required for transport (ESCRT) complex.

CONCLUSIONS. *S. pneumoniae* releases sufficient amounts of pneumolysin to perforate the plasmalemma of host cells, however, the immediate cell lysis, which is frequently reported as a result of treatment with purified and artificially concentrated toxin, appears to be an unlikely event *in vivo* since the toxin pores are efficiently eliminated by microvesicle shedding. Therefore the dysregulation of cellular homeostasis occurring as a result of transient pore formation/elimination should be held responsible for the damaging toxin action.

GENERAL SIGNIFICANCE. We have achieved a comprehensive view of a general plasma membrane repair mechanism after injury by a major bacterial toxin.

1. Introduction

Streptococcus pneumoniae is a potent human pathogen. Infection leads to common diseases such as otitis media, meningitis and pneumonia, which affect several million people and is responsible for significant infant death in developing countries [1]. The bacterial exotoxin pneumolysin (PLY) is instrumental for the breach of epithelial and endothelial barriers and the incapacitation of the host's immune system [2, 3].

PLY belongs to the large family of cholesterol-dependent cytolysins (CDC), toxins that are structurally related and characterized by their large trans-membrane pore [4]. Other prevalent pathogens producing CDCs are *Streptococcus pyogenes* (streptolysin O, SLO) and numerous other Gram positive bacteria, such as *Clostridium, Listeria* and *Bacillus* [5]. During the progress of infection PLY is released by the bacteria as soluble monomers that bind to cholesterol-rich microdomains within the plasma membrane of the host cells [2, 6]. After binding, PLY assembles in circular oligomeric prepores, undergoes a conformational change and perforates the plasmalemmal lipid bilayer. The formation of transmembrane pores leads to the loss of plasmalemmal integrity that might result in the lysis of targeted cells and ultimately in extended tissue damage at the site of infection and overwhelming immune responses [2].

However, plasmalemmal perforation by pore-forming toxins does not necessarily entail an unfavourable prognosis with respect to cellular survival. Largely depending on the concentration of a pore-forming toxin, the repertoire of cellular responses is considerable and ranges from the activation of intracellular and transmembrane signaling cascades i.e. for the initiation of the release of cytokines at non-lytic toxin concentrations, to imminent lytic cell death at lytic ones [2, 7, 8].

Lytic cell death has frequently been documented by using purified, concentrated exotoxins [2, 7]. Recently, we have shown that even at non-lytic concentrations of purified PLY the majority of targeted host cells are being perforated; however, these injuries are rapidly and efficiently resealed [9]. Ca^{2+}-dependent recruitment of the repair machinery leads to plugging

of toxin pores that are either expelled into the extracellular space or internalized into the cellular interior [7, 10-12].

Here we show that during their growth bacteria produce enough PLY to perforate the plasma membrane of human cells. However, the host cells are capable of efficiently eliminating the active toxin pores and thus do not succumb to lytic death. Evaluating the mechanisms that are responsible for the elimination of toxin pores, we show that they are actively ejected and that both prepores and functional toxin pores are expelled in a Ca^{2+}-triggered mechanism. Individual toxin pores and prepores have been identified by cryo-electron microscopy. Mass spectrometry results demonstrate that microvesicles are highly enriched in PLY, annexins, actin-binding and Ca^{2+}-regulated proteins and that they also contain components of the ESCRT machinery.

2. Materials and methods

2.1. Mammalian cell culture and transfections

Human embryonic kidney cells (HEK 293) and neuroblastoma SH-SY5Y cells were cultured as described [13]. HeLa cells were maintained in DMEM (Dulbecco`s modified Eagle`s medium. Gibco, Life Technologies, Paisley, UK) supplemented with 10% heat-inactivated FBS (Fetal Bovine Serum. Gibco, Life Technologies, Paisley, UK) and 1% penicillin-streptomycin (Gibco, Life Technologies, Paisley, UK). Cell cultures were grown in 5% CO_2 at 37°C. Transfections were performed as described in [14]. Cells were transiently transfected with the coding sequence of human annexin A2, A6 or porcine annexin A1 cloned into the Living Colors Fluorescent protein vector pEYFP-N1 (Takara Bio Europe/Clontech, Saint-Germain-en-Laye, France) [14] and/or with a human charged multivesicular body protein 4B (Chmp4B)-mCherry construct [15]. Transfected cells were seeded on coverslips and were incubated for 48 h, reaching 80-90% confluence. The transfection rate for the fluorescently-labeled constructs ranged between 70 - 90%.

2.2. Bacterial cultures

The clinical pneumococcal isolates were collected in Switzerland from 1-10 year old children of both sexes. Strains 103.57, 211.25, 109.74, 307.14, 207.06, 208.41, 106.66, 207.31 and 202.67 were from nasopharyngeal swabs (otitis), whereas strains B101.77, B103.21 were from blood cultures (septicemia). The clinical pneumococcal isolates as well as the pneumococcal strains D39 and PLN-A (D39 deficient in expressing PLY) were cultured in BHI (Brain Heart Infusion Broth, Sigma Aldrich, Buchs, Switzerland) at 37°C. The PLN-A strain carries an erythromycin resistance marker [16], therefore the medium was supplemented with 1 µg/ml erythromycin (Sigma Aldrich). For the generation of bacterial supernatants, bacteria grown to their stationary phase (OD_{500} = 1.0) were pelleted (5,000 x g) for 15 min. The supernatants were filtered through a syringe filter with a pore size of 0.2 µm (VWR, Dietikon, Schweiz). Overnight cultures from D39 strain used for co-culturing experiments were diluted to OD_{500} = 0.01 in DMEM medium supplemented with 10% heat-inactivated FBS and 20 mM HEPES (Merck, Zug, Switzerland) and grown to early stationary phase. For the establishment of growth curves, the overnight cultures were diluted to OD_{500} = 0.01 and the OD_{500} was measured every 1.5 h.

2.3. Recombinant toxins

The nontoxic PLY mutant ΔA146R147 exhibits a double-amino acid deletion within the PLY sequence [17] and is N-terminally tagged with GFP. Recombinant PLY and EGFP-tagged PLY were cloned and purified as follows: all primers were synthesized by Microsynth (Balgach, Switzerland) and are detailed in the Supplementary File 1. Restriction enzymes were from Fermentas (ordering partner: Fisher Scientific, Wohlen, Switzerland) and all other reagents used in the cloning experiments were purchased from Promega (Dübendorf, Switzerland) if not otherwise stated. Isolation of the genomic DNA of the strain D39 was performed with the E.Z.N.A. ® Bacterial DNA Kit (VWR). The PLY gene and the EGFP gene (from pN1-EGFP vector; Clontech, Saint-Germain-en-Laye, France) were amplified. The PCR products as well as the pET28a vector were cut with the complementing restriction

5

enzymes (BamHI, XhoI) and purified by the PCR Clean-up Kit (Qiagen, Hilden, Germany). First the PLY PCR product was ligated into the pET28a vector (Novagen, Madison, USA; digested with BamHI and XhoI). Subsequently, the EGFP PCR-product was ligated into the pET28a-PLY vector (digested with NheI and BamHI) by the T4-DNA ligase. Positive clones were sequenced. The pET28a-PLY and the pET28a-EGFP-PLY vector were transformed in BL21 (DE3) pLysS competent cells. Protein expression was induced with 1 mM IPTG (Sigma Aldrich) at the bacterial culture OD_{500} = 0.5 - 0.7. Bacterial cells were incubated for 4 h at 37°C and harvested by centrifugation (5,000 x g, 4°C, 30 min). The recombinant proteins were purified with Protino® Ni-NTA 1 ml columns (MACHEREY-NAGEL, Oensingen, Switzerland) according to the manufacturer`s instructions. The protein content of the eluates was determined by sodium dodecyl sulfate polyacrylamide gel electrophoresis (SDS-PAGE) and high protein contents were pooled. Two dialysis steps to phosphate buffered saline (PBS) (1 mM DTT added) were performed with a cellulose membrane tube that retains proteins with ≥ 12 kDa (Sigma Aldrich) according to the manufacturer`s instructions. The protein concentration was determined with a bicinchoninic acid (BCA) assay (Pierce™ BCA Protein Assay Kit, Thermo Scientific, Reinach, Switzerland) and the hemolytic activity of PLY as well as EGFP-PLY was assessed by a hemolysis assay.

2.4. Hemolysis assay

Human red blood cells were isolated from whole blood of healthy volunteers and were stored in the Alsever's solution (Sigma Aldrich). Before each experiment red blood cell suspension was centrifuged (3,000 x g, 4°C, 10 min). Pelleted erythrocytes were washed twice with PBS (3,000 x g, 4°C, 10 min) and used as the source (100%) in the hemolysis assay. Serial dilutions of bacterial culture (OD_{500} = 1.0) supernatants or recombinant toxins, pre-activated with 5 mM DTT, were incubated with 1 % human red blood cells at 37°C for 60 min in PBS. The absorbance of the supernatant was measured at 450 nm and the hemolytic activity was calculated according to the formula: hemolysis (%) = ((A $_{sample}$ − A $_{negative\ control}$) / (A $_{positive\ control}$ −

A $_{negative\ control}$)) x 100. Negative control = 1 % human red blood cells in PBS. Positive control = 1 % human red blood cells in H_2O.

2.5. Confocal microscopy

If not otherwise stated Tyrode`s buffer (140 mM NaCl, 5 mM KCl, 1 mM MgCl2, 10 mM glucose, 10 mM HEPES, pH = 7.4) containing 2.5 mM $CaCl_2$ (calcium Tyrode`s buffer) or 100 µM EGTA was used in all experiments. Imaging was performed as described in [9]. In brief, transfected cells (~250000 cells/coverslip) were mounted in a recording perfusion chamber and were washed with 200 µl of Tyrode`s buffer containing calcium or EGTA. At time point = 0 the buffer was completely removed and the cells were treated with 200 µl of the indicated solutions. If mammalian cells were treated with bacterial supernatants, 100 µl of bacterial supernatants were diluted in 100 µl calcium Tyrode's buffer. Co-culturing of mammalian cells with *S. pneumoniae* was performed as follows: transfected HEK 293 cells were grown to confluency in cell culture dishes with a glass bottom (CELLviewTM, Ø35 mm, Greiner Bio-one, Frickenhausen, Germany). Mammalian cells were washed with calcium Tyrode`s buffer, infected with 2 ml of bacterial culture (OD_{500} = 0.4) and monitored for 80 min at 37°C and 5% CO_2. Fluorescence was recorded in time series for 45 min with an Axiovert 200 M microscope equipped with a laser scanning module LSM 510 META (Zeiss) using a x63 oil immersion lens [18]. Annexin-A2 positive microvesicles that were released in individual experiments were counted manually (every 5th frame, 300 frames à 9 s) and are expressed as the number of microvesicles/cell/min.

2.6. Isolation of PLY-induced microvesicles and total membrane isolates

HEK 293 cells (10^7 cells, transfected or untransfected as indicated) were gently washed with PBS. Microvesicle shedding was induced by treatment with PLY or EGFP-PLY in calcium Tyrode`s buffer containing 5 mM DTT (2 µg/ml PLY in 2 ml total volume). If indicated, the unbound toxin was removed after 2.5 min and the toxin-free calcium Tyrode`s buffer was re-added. The cells were incubated for 45 min at room temperature. The supernatant containing

the shed microvesicles was collected. Total membranes were isolated by detaching cells with a cell scraper and rigorous fragmentation (20 x) with a glass homogenizer. The supernatant containing shed microvesicles or the fragmented cell suspension was centrifuged two times at 2,100 x g for 10 min to remove cell debris and membrane material was pelleted at 130,000 x g for 1h (90TI rotor, Optima L, Beckman Coulter, Nyon, Switzerland). The pellets were re-suspended in calcium Tyrode`s buffer (for cryo-electron tomography) or 1 x SDS sample buffer for SDS-PAGE.

2.7. Mass spectrometry

The microvesicle and the total membrane pellets were subjected to SDS-PAGE (the total membrane isolate was loaded in x 2 serial dilutions). After Coomassie Brilliant Blue R-250 staining (Sigma-Aldrich), the microvesicle isolate lane and the total membrane isolate lane containing the matching protein concentration were carefully dissected out and analyzed by the Mass Spectrometry and Proteomics Core Facility (PMSCF) of the Department of Clinical Research at the University of Bern with an ESI-LTQ-Orbitrap: The samples were reduced, alkylated and digested with trypsin. Each sample was loaded onto a pre-column (PepMap C18, 5µm, 300A, 300µm x 1.5mm length) at a flow rate of 20µL/min with solvent A (0.1% formic acid in water/acetonitrile 98:2). After loading, peptides were eluted in back flush mode onto the analytical nano-column (magic C18, 5µm, 300A, 0.075 mm i.d. x 75mm length) using an acetonitrile gradient of 5% to 40% solvent B (0.1% formic acid in water/acetonitrile 4,9:95) in 60min at a flow rate of ~400nL/min. The column effluent was directly coupled to an LTQ-orbitrap XL mass spectrometer (ThermoFisher, Bremen, Germany) via a nano spray ESI source operated at 1700 V. Data acquisition was made in data dependent mode with precursor ion scans recorded in the Fourier transform detector (FT) with resolution of 60'000 (@ m/z =400) parallel to five fragment spectra of the most intense precursor ions in the linear iontrap. CID mode settings were: Wideband activation on; precursor ion selection between m/z range 360-1400; intensity threshold at 500; precursors excluded for 15 sec. CID spectra interpretation was performed with EASYPROT on a local, multicore processor server run

8

under linux. A small database containing all UniProt database: uniprot_sprot; taxonomies: 1313, 9606. The following variable modifications were used: carboamidomethylated Cys (no limit), Met oxidation (limited to 1), Asn/Gln deamidation. 2. Parent and fragment mass tolerances were set to 10 ppm and 0.6 Da, respectively.

All peptides identifications with a score of >4 were accepted for peptide mapping. The protein match score summation (PMSS) was used for relative quantification [19]. The PMSS adds up all scores from peptide spectral matches to one particular protein irrespective of whether a peptide was identified several times, with or without modifications.

2.8. Immunoblotting / amido black staining

The pellet of microvesicles as well as the total membrane pellet (in x 2 serial dilutions) was applied to SDS-PAGE. Immunoblotting was performed with a polyvinylidene difluoride (PVDF) membrane (Millipore AG, Zug, Switzerland) and a mouse monoclonal antibody against annexin A2 (#A14020, BD Biosciences, Allschwil, Switzerland), annexin A6 (#610067, BD Biosciences, Allschwil, Switzerland) and heat shock protein 90 (Hsp90) (#SMC-149 A/B, StressMarq Biosciences Inc., Victoria, Canada). All 1st antibodies were diluted 1:500. The horseradish peroxidase (HRP)-linked ECL 2nd antibody was diluted 1:1000 (#NA931-1ML, GE healthcare, Little Chalfont, UK). The membrane was developed with WesternBright ECL (Advansta, Menlo Park, USA) and the band intensities were analyzed by FIJI [20]. After immunoblotting, the membrane was stained with amido black and the relative total protein content in the microvesicle sample was determined by matching to serial dilutions of the total membrane isolates. In addition, the protein concentration of the microvesicle isolate and the total membrane isolate was determined by a BCA assay.

2.9. Fluorescence activated cell sorting (FACS) analysis

PLY or EGFP-PLY induced microvesicles shed from either annexin A2-mCherry or non-transfected HEK 293 were isolated by centrifugation as described above and re-suspended in equal volumes for FACS analysis (400 µl). For FM1-43 (SynaptoGreen C4, Biotium,

9

Hayward, USA) staining the microvesicles were incubated with 12.3 µg/ml dye. The mixture was shortly vortexed, incubated for 10 min and directly subjected to FACS measurement. Microvesicles were analyzed with a LSRII (BD Instruments, San Jose, USA). The settings and compensations were set according to microvesicles from non-transfected cells induced by PLY, non-transfected cells induced by PLY-EGFP, and annexin A2-mCherry transfected cells with PLY. Data acquisition was performed with constant sample flow rate and was analyzed with FlowJo software (FlowJo, LLC, Ashland, USA). Data acquisition was performed with constant sample flow rate and was analyzed with FlowJo software (FlowJo, LLC, Ashland, USA).

2.10. Immunogold labeling and conventional electron microscopy

The supernatant of PLY-challenged HEK 293 cells was centrifuged two times at 2100 x g for 10 min and filtrered (syringe filter, PFTE membrane, pore size 0.45 µm, Millex, Millipore). The membrane was removed from the plastic housing, cut into individual segments and incubated with a mouse monoclonal antibody against PLY (PLY-4, 1:50; Abcam, Cambridge, UK), washed with Tyrode`s buffer containing 2.5mM Ca^{2+} followed by incubation with an IgG goat anti-mouse 10 nm gold 2nd antibody (1:100; Sigma-Aldrich). The membrane was frozen at high pressure (210 MPa, EMPACT instrument, Leica-Microsystems, Vienna, Austria), cooled down to -196 °C and freeze-substituted as described previously in [21]. Ultrathin sections were viewed with a Philips CM12 transmission electron microscope and images were recorded with the Olympus analySIS software (Olympus, Volketswil, Switzerland).

2.11. Cryo-electron tomography

Isolated microvesicles were mixed with 10 nm fiducial gold solution (#s10110/8, AURION Immuno Gold Reagents & Accessories, Wageningen, The Netherlands). The mixture was applied to a 200 mesh lacey carbon film grid (#AGS166-3, Agar Scientific, Elektron Technology UK Ltd, Stansted, UK). Excess liquid on the grid was removed by blotting with a filter paper and the grid was immediately plunge frozen in liquid ethane with a homebuilt

plunge freezer. The grid was mounted on a cryo-holder (Gatan, Pleasonton, CA, USA) and transferred to a Tecnai F20 transmission electron microscope (FEI, Eindhoven, The Netherlands), set to low dose conditions, operated at 200 kV, and equipped with a field emission gun. Images were recorded with a 2k x 2k charge-coupled device (CCD) camera (Gatan) mounted after a GIF Tridiem post-column filter (Gatan) operated in zero-loss mode. The sample was kept at about -180°C. Tilt series were acquired using SerialEM for automated acquisition recorded typically from -60° to 60° with a 2° angular increment. Defocus was set to -8 μm and the total electron dose used was about 90 e-/$Å^2$. Image processing was done in IMOD [22]. The alignments were done using the automated fiducial tracking function and the 3D reconstructions were done using the weighted back projection followed by a nonlinear anisotropic diffusion (NAD) filtering.

3. Results

3.1. Plasmalemmal repair in host cells damaged by *S. pneumoniae*

In nucleated cells, PLY-induced plasmalemmal perforations lead to a pore-induced entry of extracellular Ca^{2+} [14]. As a result, fluorescently-labelled annexin A2 (used as an intrinsic Ca^{2+} sensor [14]) translocated from the cytoplasm to the plasma membrane (Supplementary Figure 1A, B, cells marked by stars, Video 1, 2). Ongoing plasmalemmal repair and the elimination of PLY-pores manifested themselves by annexin A2 back-translocation to the cytosol as a result of plasmalemmal resealing and the restoration of $[Ca^{2+}]_i$ to its resting levels by the cellular Ca^{2+}-sequestration machinery [9] (Supplementary Figure 1A, Video 1). Failure to reseal the damaged plasmalemma led to lysis of the affected cells [9, 18]. Equilibration between extracellular (~2.5 mM) and intracellular (~100 nM) $[Ca^{2+}]$ resulted in stable elevation of $[Ca^{2+}]_i$ followed by the permanent association of annexin A2, with the plasmalemma and, at a later stage, also with intracellular membranes (Supplementary Figure 1B, Video 2). Supplementary Figure 1 and Videos 1 and 2 show results of experiments performed in HEK 293 cells that were treated with a *S. pneumoniae* bacterial culture supernatant; similar results were obtained with purified PLY [9] and SLO [13]. Identical responses to permeabilization by pore-forming toxins were observed in primary human airway epithelial cells (AEC), human neuroblastoma SH-SY5Y cells and human bronchial epithelial cells (HBE) [9, 13]. This suggests that the elimination of toxin-induced pores is a general cellular defense mechanism which is independent of cell- or toxin type.

In order to ascertain PLY concentrations ([PLY]) that are required for the perforation/lysis of nucleated cells, monolayers (80-90 % confluence) of epithelial (HEK 293) or mesenchymal (SH-SY5Y) cells, expressing annexin A2-YFP, were treated with varying amounts of purified PLY. Infrequent plasmalemmal perforations were registered already at [PLY] = 50 ng/ml (~1 nM) (not shown); at 250 ng/ml [PLY] ~30% of cells, and at 1 µg/ml [PLY] ~60% of cells were permeabilized (Figure 1). No differences in the extent of plasmalemmal perforation were observed between HEK 293 and SH-SY5Y cells (Figure 1).
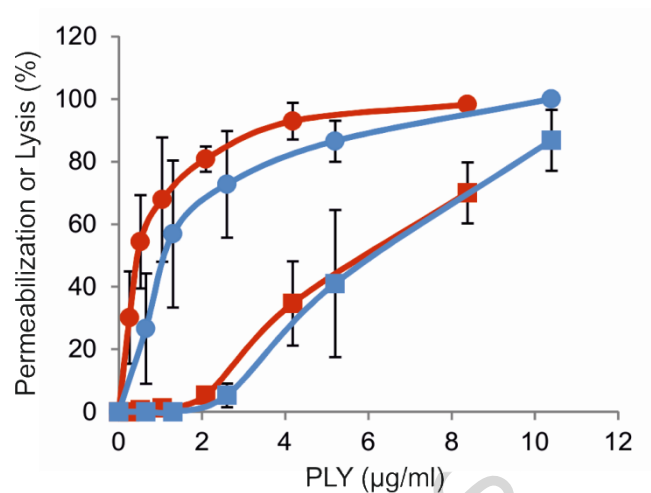
Figure 1

Figure 1: Permeabilization and lysis of nucleated cells by purified PLY.

HEK 293 cells (red lines) or SY5Y cells (blue lines) were treated with different [PLY]. The percentage of cells showing plasmalemmal perforation (circles) and lysis (squares) are plotted. The 1 µg/ml point corresponds to 87 hemolytic units. Mean ± SD, N ≥ 6;

Nucleated cells have developed the means of repairing pore-induced plasmalemmal lesions ([7]; Supplementary Figure 1A, Video 1). Hence, in comparison to their degree of plasmalemmal perforations, much higher [PLY] (≥ 2 µg/ml) were required to induce cell lysis (Figure 1). There was no difference in the extent of PLY-induced lysis between HEK 293 and SH-SY5Y cells (Figure 1).

In order to ascertain whether [PLY] that are required for the perforation/lysis of nucleated cells can be reached in pneumococcal cultures, i.e. at conditions that are likely to occur *in vivo*, [PLY] were estimated in 11 clinically isolated *S. pneumoniae* strains and in the D39 laboratory strain by comparing their hemolytic activity with that of purified PLY of known concentration (Table 1). Two of the tested strains showed no hemolytic activities, which suggests that these strains do not express/release PLY. Among the hemolytically active strains, [PLY] in the bacterial culture supernatants ranged from 200 ng/ml to 800 ng/ml. Notably, whereas all hemolytically active strains produced PLY at concentrations that were

13

sufficient to permeabilize nucleated cells, none of the strains seem to release enough PLY to induce lysis of the cells as judged from indirect comparison of data obtained in hemolysis assay (Table 1) and in experiments performed in nucleated cells (Figure 1).

Table1: Concentration of PLY in S. pneumoniae strains. [PLY] released by 12 S. pneumoniae strains were determined by comparing the hemolytic activities of bacterial culture supernatants with that of purified PLY of known concentration. One hemolytic unit will cause 50% lysis of 1% red blood cell suspension in phosphate buffered saline, pH 7.4, after incubation at 37 °C for 60 min. Mean ± SD, N = 6.

S. *pneumoniae* (strain)	[PLY] (µg/ml)	Hemolytic activity (Units/ml)
103.57 (nasopharyngeal swab)	0.799 ± 101	333
211.25 (nasopharyngeal swab)	0.641 ± 181	263
109.74 (nasopharyngeal swab)	0.629 ± 169	262
307.14 (nasopharyngeal swab)	0.439 ± 86	200
207.06 (nasopharyngeal swab)	0.419 ± 81	175
208.41 (nasopharyngeal swab)	0.371 ± 185	156
106.66 (nasopharyngeal swab)	0.343 ± 66	143
B101.77 (blood culture)	0.248 ± 14	103
D39	0.217 ± 28	90
207.31 (nasopharyngeal swab)	0.199 ± 36	83
B103.21 (blood culture)	0	0
202.67 (nasopharyngeal swab)	0	0
		(Units/mg)
Purified PLY	4000	435000

Purified eGFP-PLY	2000	250000

In order to address the permeabilization/cytolytic activities of pneumococcal culture supernatants directly in nucleated cells, HEK 293 and SH-SY5Y cells expressing annexin A2-YFP were treated with bacteria-free culture supernatants obtained from *S. pneumoniae* D39 or *S. pneumoniae* 103.57 strains. D39 was among the strains that released the lowest amount of PLY, whereas 103.57 released the highest amount of PLY (Table 1). Pneumococci predominantly release PLY when they reach the stationary phase of growth and undergo autolysis [23, 24]. At these conditions (stationary phase; $OD_{500}=1.0$) the perforation of nucleated cells was minimal for the D39 bacterial strain (HEK 293 cells: 8% ± 5% SD, total of 107 cells recorded in 4 separate experiments; SH-SY5Y cells: 8% ± 8% SD (total of 70 cells recorded in 3 separate experiments) and no lysis of either HEK 293 or SH-SY5Y cells was observed.

In order to ensure that PLY activity was not lost during the preparation of bacterial culture supernatants, we performed co-culture experiments, in which D39 bacteria grown to late-exponential-phase in DMEM cell culture medium ($OD_{500}=0.4$), were directly applied to HEK 293 cells and were further co-incubated with the cells for 80 minutes reaching the stationary phase of growth ($OD_{500}=0.5$, Supplementary Figure 2). Comparable to the experiments with bacteria-free culture supernatants, 8% ± 8% SD of cells (total of 215 cells recorded in 5 separate experiments) experienced plasmalemmal perforations during co-culturing with D39 bacteria; all were able to reseal their PLY-damaged plasmalemma (Video 3).

Next, we treated nucleated cells with the bacterial culture supernatant obtained from *S. pneumoniae* 103.57 strain, which was the most hemolytically active one among all bacterial strains that were tested in this study (Table 1). Even at these experimental conditions only 49% ± 10% SD of HEK 293 cells (220 cells in 5 separate experiments) were permeabilized, and a mere 2% ± 3% SD succumbed to PLY-induced lysis. Similar results were obtained with SH-SY5Y cells: 43% ± 20% SD of cells treated with the 103.57 supernatant (total of 112 cells

recorded in 5 separate experiments) experienced plasmalemmal perforations; all perforated cells were able to reseal.

Despite its prominent binding to the plasmalemma, the inactive fluorescently-labelled PLY mutant ΔA146R147 [17] did not trigger plasmalemmal perforations in HEK 293 cells as judged by the absence of annexin A2 translocations (Video 4). Likewise, stationary, PLY-deficient PLN-A bacteria, in which PLY is genetically disrupted were unable to induce annexin A2 translocations [16] (Video 5).

Taken together, these experiments suggest that *in vivo,* pneumococci are able to produce sufficient PLY to perforate the plasmalemma of host cells; however the cells possess adequate means to repair such plasmalemmal injuries - at least at the initial stage of pneumococcal infection.

3.2. Mechanisms of plasmalemmal repair: annexin- and PLY-containing microvesicles are shed by cells treated with *S. pneumoniae*

We have shown that members of the annexin protein family are instrumental in the repair of toxin-induced pores [7, 25]. By translocating to the perforated plasma membrane the annexins plug the pores that are subsequently expelled into the extracellular space [9, 13, 21]. Accordingly, the plasmalemma of nucleated cells treated with *S. pneumoniae* 103.57 culture supernatants (Figure 2A, B) or with sub-lytic concentrations of purified PLY (Figure 2C) sprouts thin, annexin A2-YFP positive "nanotubes" (Figure 2 arrows) that appear to break down by releasing microvesicular material into the extracellular milieu (Figure 2 arrowheads, Video 1). The annexin A2 plugs are marked by stars (Figure 2 B; C). Likewise, protrusions were generated and microvesicles were released by HEK 293 cells after ~ 60 minutes of co-culturing with *S. pneumoniae* D39 (Video 3) or after treatment with sub-lytic [PLY] (Video 6).
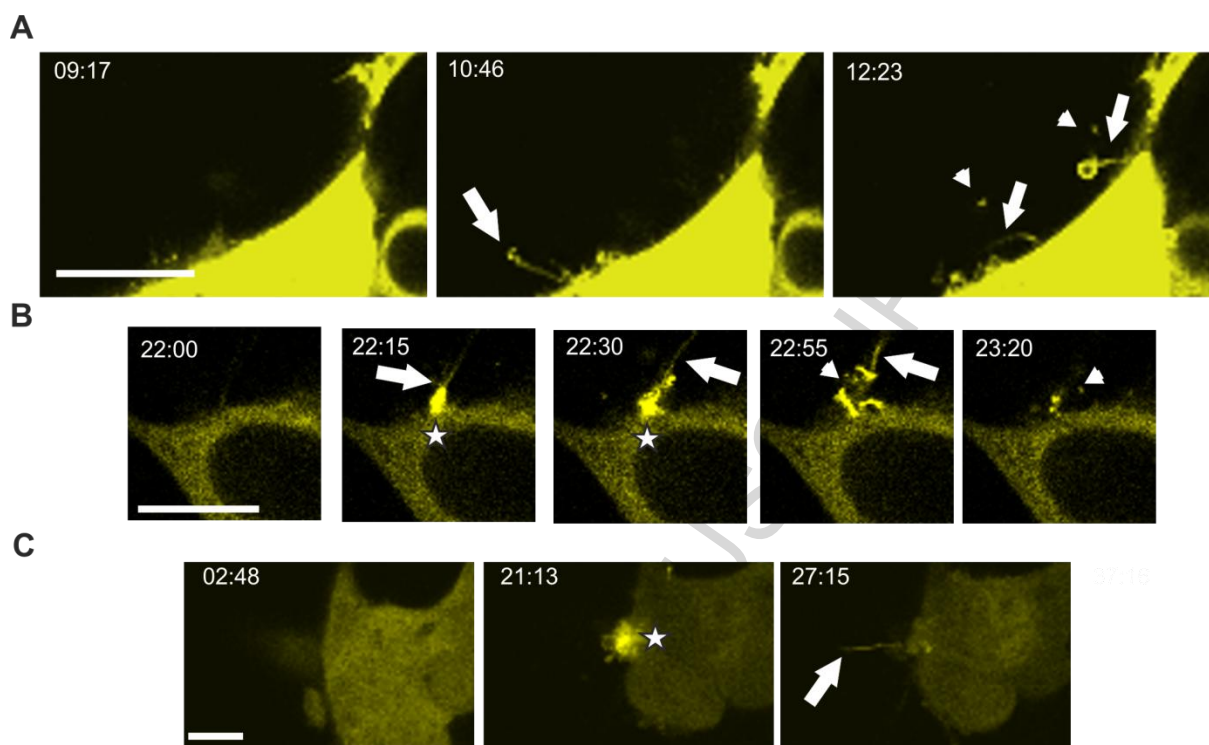
16

Figure 2

*Figure 2: PLY-induced formation of nanotubes and release of microvesicles in HEK 293 and SH-SY5Y cells. The 103.57 pneumococcal supernatant (67 hemolytic units) initiates sprouting of thin nanotubes from the plasma membrane of HEK 293 (**A**, arrows) or of SH-SY5Y (**B**, arrows) cells. Their breakdown is followed by the ejection of microvesicles (arrowheads). Purified PLY (2 µg/ml; 174 hemolytic units) also induces nanotube formation, which is accompanied by the subsequent release of microvesicular material (**C**). Representative images are shown. N = 5. Min:sec = time after treatment with the bacterial supernatant. Scale bars = 10 µm*

Released microvesicles contained membrane-associated annexins but were completely devoid of cytosolic proteins (Figure 3, Video 6), which suggests that the formation of an outward plasmalemmal fold composed of two tightly associated lipid bilayers is involved in shedding of the toxin.

17
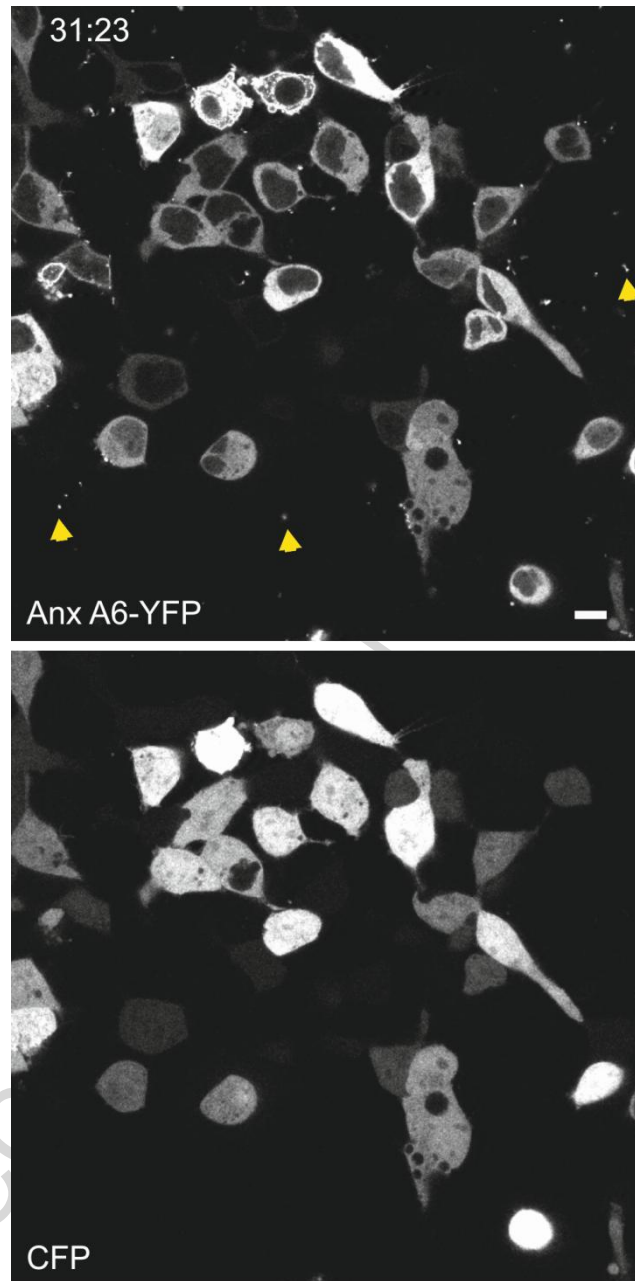
Figure 3

Figure 3: Annexin-rich microvesicles are devoid of cytosolic CFP. *Sub-lytic [PLY] (2 μg/ml;*

174 hemolytic units) induce the release of annexin A6 containing microvesicles (upper panel,

examples are highlighted by yellow arrowheads) in HEK 293 cells expressing annexin A6-

YFP and cytosolic CFP. Similar results were obtained also for other annexins (annexin A2

and annexin A1). However, the shed microvesicles do not contain CFP (lower panel). N = 3.

Representative images are shown. Min:sec = time after treatment. Scale bar = 10 μm.

For the unequivocal detection of PLY on the plasma membrane we generated hemolytically active, N-terminally EGFP-tagged PLY. The labelled toxin enabled us to observe the formation of nanotubes and the release of microvesicles that contained both annexin A2 and PLY (Figure 4).
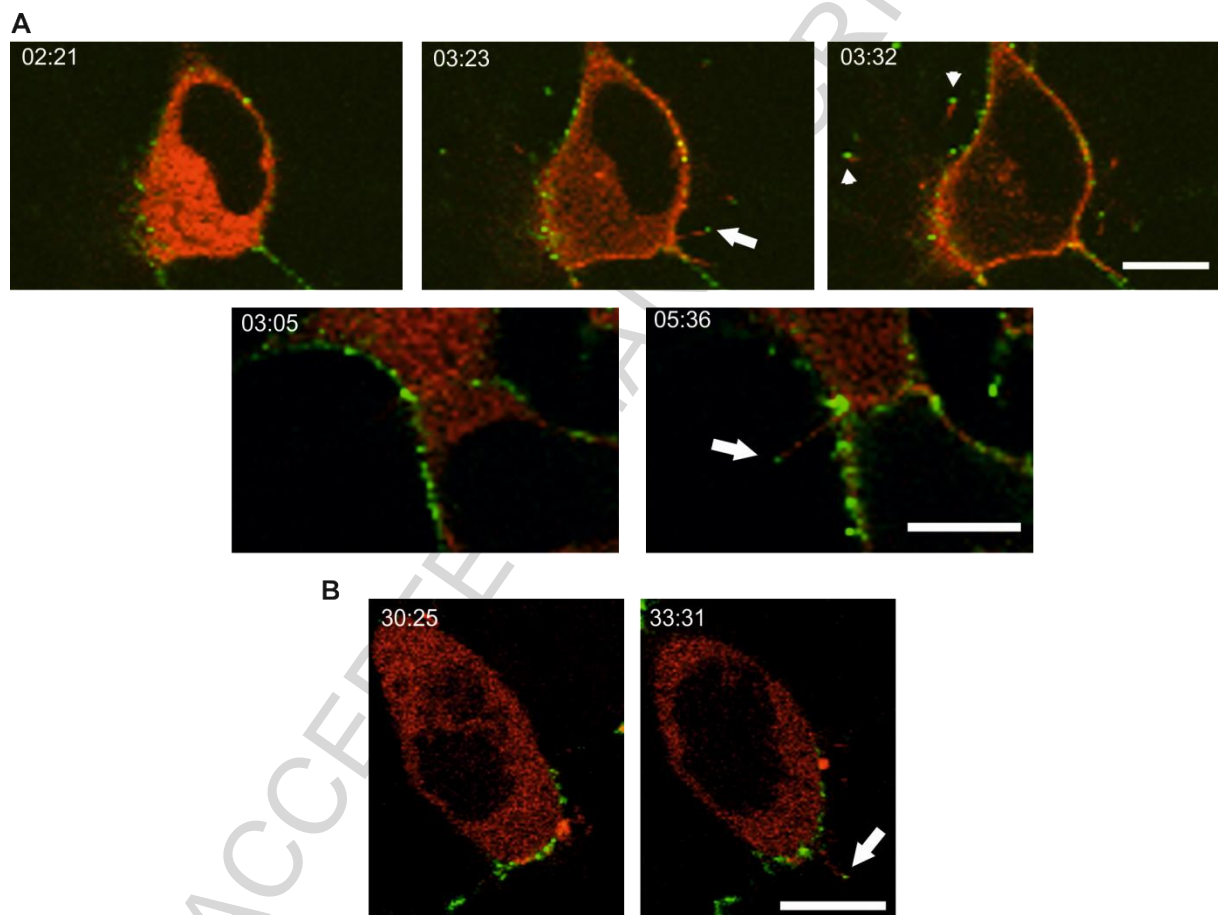
Figure 4

Figure 4: Formation of nanotubes and release of microvesicles visualized with EGFP-PLY. Annexin A2-mCherry-expressing SH-SY5Y (A) or HEK 293 (B) were treated with 2 μg/ml EGFP-PLY (100 hemolytic units). EGFP-PLY rapidly binds to the plasma membrane and initiates the formation of nanotubes with the toxin capping their tips (arrows) and the release of microvesicles (arrowheads). N = 4. Representative images are shown. Min:sec = time after treatment. Scale bars = 10 μm.

FACS analysis of microvesicles isolated from annexin A2-mCherry transfected HEK 293 cells confirmed the co-localization of EGFP-PLY with the annexin (Supplementary Figure 3). Despite a caveat of underrepresenting a population of microvesicles that were smaller than 500 nm, these data corroborate our imaging results (Figure 4) and are consistent with our previous suggestion that the removal of PLY pores from the plasmalemma during repair occurs by a process of annexin-mediated plugging and shedding [13, 21].

The presence of PLY on shed microvesicles was additionally confirmed by immunogold labelling with toxin-specific antibodies (Supplementary Figure 4).

The internalization of toxin pores following lysosome-plasmalemma fusion constitutes an alternative mechanism for repair of toxin-damaged plasmalemmal regions [26]. However, we were unable to detect an internalization of EGFP-tagged PLY in SH-SY5Y or HEK 293 cells either at sub-lytic [PLY] (Figure 4) or at lytic [PLY] (Supplementary Figure 5).

Toxin-induced nanotube formation in artificial membranes [27] and the formation of SLO-containing ectosomes/blebs in PFA-fixed cells [28] suggest that plasmalemmal tubulation and shedding might occur spontaneously, as a result of an intrinsic lipid rearrangement within the toxin-targeted plasmalemmal lipid-bilayer. Those studies imply that shedding follows in a protein-independent manner and therefore also occurs in lysed cells. However, our results indicate that microvesicles are preferentially shed at sub-lytic [PLY] by actively repairing cells: a peak of microvesicle release was observed at 2 µg/ml PLY (Figure 5) - at conditions when ~70% of the cells were permeabilized but successfully resealed their plasmalemma and only ~ 5% were undergoing lytic degradation (Figure 1, Video 7; [9]).
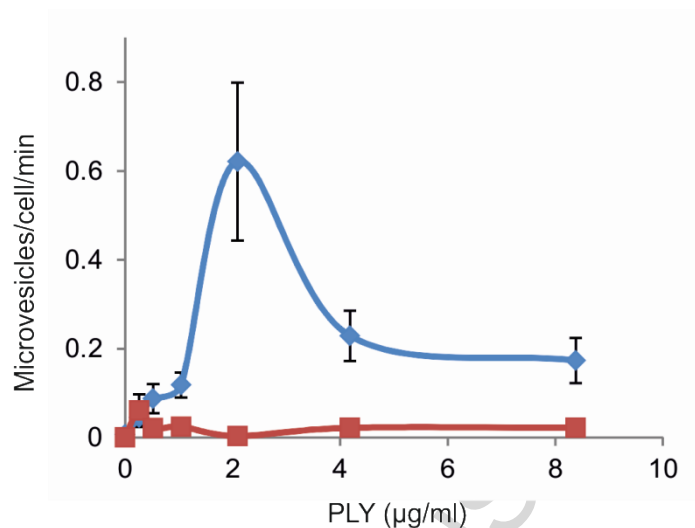
Figure 5

Figure 5: Microvesicles are predominantly shed at sub-lytic PLY concentrations. HEK 293 cells expressing fluorescently-labeled annexin A2 were exposed to different [PLY]. At sub-lytic [PLY] = 2 µg/ml the highest amount of annexin-enriched microvesicles was released compared to lower [PLY] = 0.25 - 1 µg/ml or higher [PLY] = 4 - 8 µg/ml (blue circles). The chelation of extracellular Ca^{2+} completely inhibited microvesicle release (red squares). The 1 µg/ml point corresponds to 87 hemolytic units. For any experimental condition N ≥ 6; mean ± SEM.

At higher [PLY], at conditions under which the majority of cells succumbed to PLY-induced lysis, microvesicle release was significantly diminished (Figure 5, Video 8). This suggests that only the living, but not the lysed cells, were able to undergo PLY-induced microvesicle-driven repair. Correspondingly, the chelation of extracellular Ca^{2+}, which leads to increased cell lysis due to the ineffectiveness of Ca^{2+}-dependent repair [9] prevented the shedding of microvesicles (Figure 5).

Components of the ESCRT machinery have recently been reported to mediate the shedding of toxin-perforated membrane sites in HeLa cells [15]. In particular Chmp4B and the ATPase Vps4 (vacuolar protein sorting 4) have been proposed indispensable for the Ca^{2+}-dependent evagination and scission of wounded membranes as microvesicles [15]. We did not observe the association of Chmp4B with the plasmalemma of PLY-perforated cells, in contrast to the

PLY-induced translocation of annexin A2 (Supplementary Figure 6). However, in our experiments we failed to achieve cytosolic localization of Chmp4B, which was reported in [15], either in HEK 293, in SH-SY5Y or even in HeLa cells that were used in [15] (Supplementary Figure 6), which might be the reason for the discrepancy between the two data sets.

3.3. PLY prepores and pores are actively released within the shed microvesicles

Our imaging experiments (Figures 2 - 4) suggest that released microvesicles are smaller than 1 µM in diameter. In addition, a release of larger vesicles, some of them in the form of plasmalemmal blebs, can be expected after toxin-induced, self-inflicted mechanical damage [13]. This process is documented in Supplementary Figure 7 (Video 9), which shows a PLY-perforated cell, whose appendage initially sprouts multiple blebs and is afterwards destroyed by its own contraction. Likewise, shedding of SLO-pores within rather larger plasmalemmal blebs/ectosomes has previously been invoked as a plasmalemmal repair mechanism [28].

Cryo-electron microscopy of plunge-frozen material, which was released by cells treated with sub-lytic [PLY] demonstrated that the population of released vesicles was highly heterogeneous, ranging from 45 nm to 1560 nm (Figure 6). However, more than 90% of the vesicles were smaller than 500 nm (median = 163 nm, 176 vesicles, Figure 6), suggesting that the contribution of larger vesicles in the shedding of PLY-pores was negligible. Whereas no quantitative analysis of size distribution was provided in [28], the reported SLO-induced blebs/ectosomes were heterogeneous in size, ranging from 200 nm to 2 µm, which is similar to the size distribution, observed in the present study.
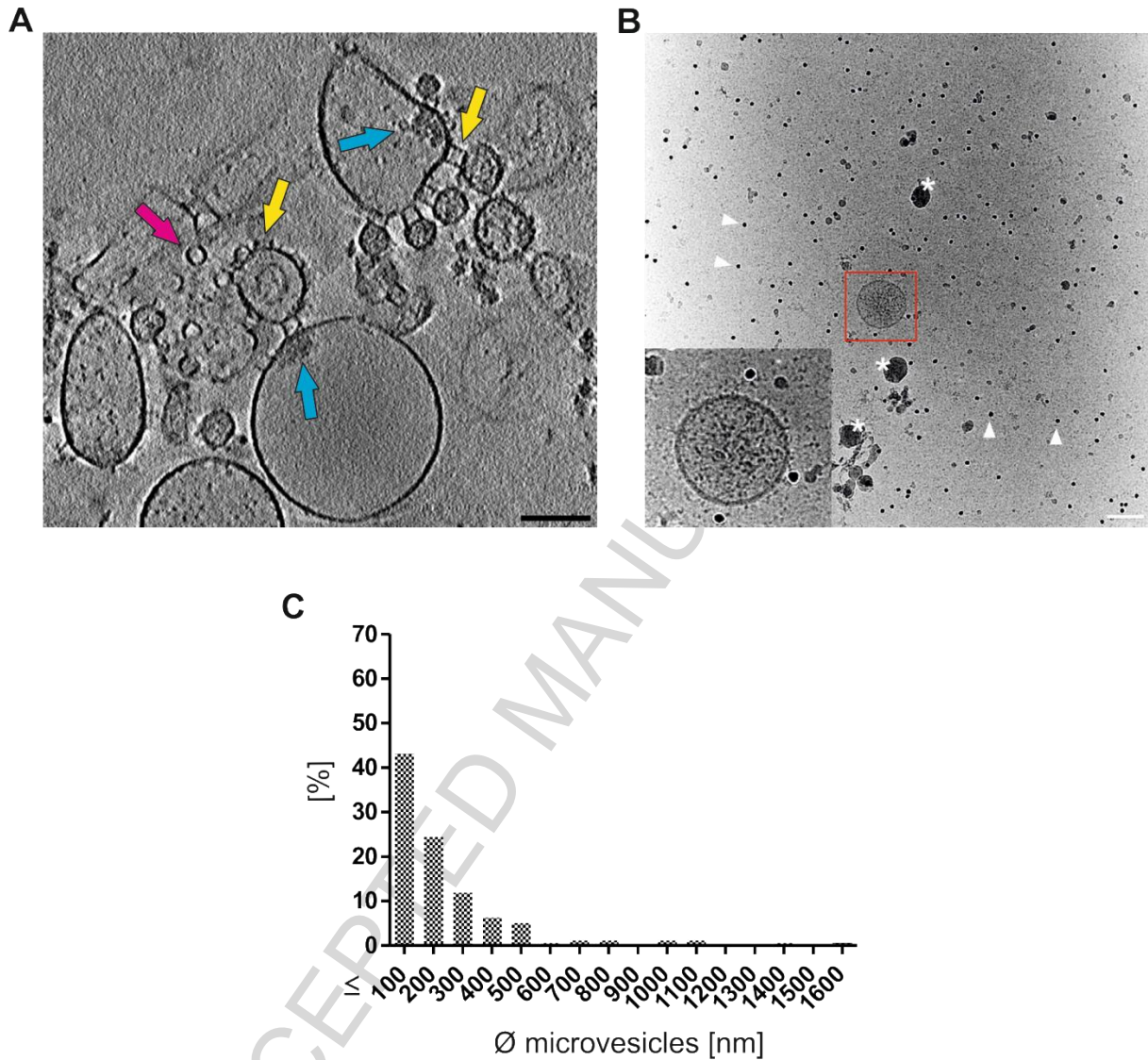
Figure 6

Figure 6: PLY-induced microvesicles visualized by cryo-EM. Sub-lytic [PLY] (2 µg/ml; 174

*hemolytic units) induce the release of microvesicles (**A**). The microvesicle population is*

heterogeneous and exhibits PLY structures bound to the membranes visible as top views

(pink arrow) and side views (yellow arrow). High density material is frequently located under

PLY structures (blue arrows). Some PLY structures associate back-to-back (upper yellow

*arrow). (**B**) A microvesicle (red square) released by cells that were not incubated with PLY.*

Only four vesicles were found on the entire EM grid (compared to ~ 10000 in case of toxin-

treated cells). Inset: magnified view of the vesicle. Asterisks: ice contamination. Arrowheads:

*fiducial gold beads. (**C**) The diameters of the microvesicles were measured in cryo-maps and*

the frequency of different sizes is given in percent. The majority of microvesicles are smaller

than 500 nm. N= 3. Scale bars = 100 nm.

Cryo-electron tomography of plunge-frozen microvesicles was further used to identify active

pores within a population of PLY that also includes prepores and PLY monomers. The side

views of PLY oligomers illustrate prepores with an intact plasma membrane underneath

(Figure 7A) as well as functional pores featuring a perforated membrane (Figure 7B). The top

view of oligomeric PLY does not allow the discrimination between prepore and functional

pore due to the inferior resolution along the Z-axis, characteristic of electron microscopic

tomography (Figure 7C).

Figure 7

Figure 7: PLY oligomers are present in the membranes of microvesicles released by HEK
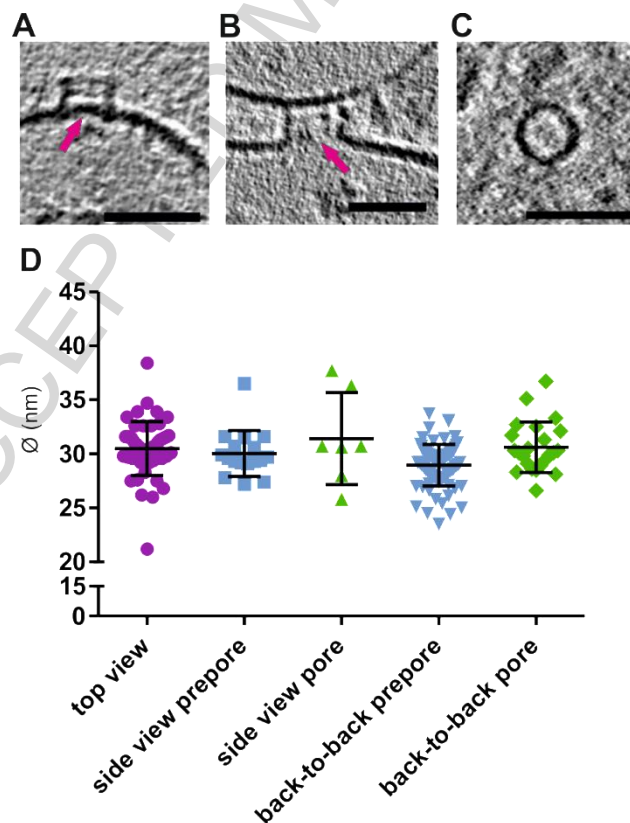
293 cells. Sub-lytic [PLY] (2 μg/ml; 174 hemolytic units) induce the release of microvesicles.

(A) PLY prepore with an intact membrane underneath the ring structure (arrow). (B) The PLY pore depicts a ruptured membrane (arrow); the pore is fused back-to-back to a prepore. (C) Top view of an assembled PLY structure. Scale bars = 50 nm. (D) The diameters of PLY-ring structures were measured in 22 tomograms. Top views (54), prepore side views (17), pore side views (7) and back-to-back structures of prepores (85) and pores (23) do not show significant differences in their ring diameters.

The diameters analyzed from the side views of prepores yield sizes in the range of 27.2 to 36.5 nm (30.0 nm ± 2.1 SD), which is similar to the size of functional pores that exhibit diameters of 25.8 - 37.7 nm (31.4 nm ± 4.2 SD) and to the diameters established in top views (21.2 - 35.2 nm; 30.0 nm ± 2.7 SD) (Figure 7D). Microvesicles are often fused by a back-to-back assembly of prepores or pores (Figure 7B), analogous to earlier reports using artificial liposomes [29].

The detection of PLY in microvesicles does not necessarily denote active toxin removal by the cell, since binding and oligomerization of PLY monomers can also occur after the microvesicles have been shed. In order to ascertain that the toxin was actively eliminated from the plasma membrane of host cells, we pre-incubated annexin A2-mCherry transfected cells with EGFP-PLY for 2.5 min which was followed by 45 min incubation in a PLY-free buffer and the isolation of microvesicles. FACS analysis revealed a population of PLY-negative, annexin-positive microvesicles in addition to microvesicles containing both PLY and the annexin (Figure 8A). The PLY-positive vesicles presumably originate from the tips of the nanotubes depicted in Figure 4 and constitute original sites of PLY-pore assembly around which the initial plasmalemmal evagination occurs. The PLY negative vesicles presumably originate from the nanotube stalks (Figure 4). Cryo-electron microscopic tomograms of microvesicles that were generated in these experiments after the unbound toxin had been removed confirms the presence of PLY pores and prepores in the membrane of shed microvesicles (Figure 8B). Quantification of the number of PLY oligomeric structures on PLY-containing microvesicles revealed an average of 21 structures per μm^2, which is

similar to the density of SLO-pores on blebs reported in [28], however, in contrast to the latter the pore:prepore ratio was estimated at 1:9.
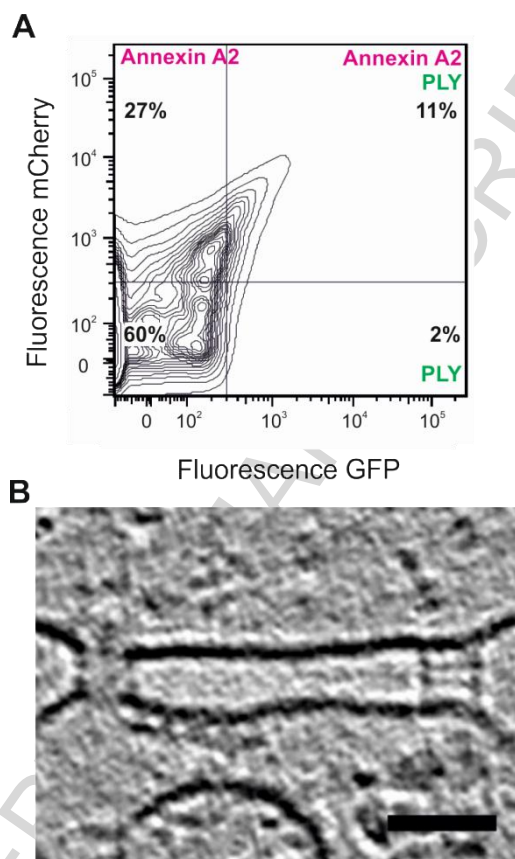
Figure 8

Figure 8: PLY structures are actively removed from the plasma membrane of host cells. HEK 293 cells expressing annexin A2-mCherry were treated with [EGFP-PLY] = 2 µg/ml (100 hemolytic units). The unbound toxin was removed after 2.5 min and cells were further incubated for 45 min.(**A**) FACS analysis of the released microvesicles revealed the presence of microvesicles containing both annexin A2 and PLY (15% ± 7% SD) as well as annexin-positive, PLY-negative (22% ± 9% SD) and a few annexin-negative, PLY-positive (1% ± 0.4% SD) microvesicles. N = 3. Data from an individual experiment with 90% transfection efficiency are shown. (**B**) Cryo-electron tomograms illustrate the presence of PLY prepores (**right side**) and pores (**left side**) in the membranes of the microvesicles. N= 5. Scale bar = 50 nm

3.4. PLY-induced microvesicles carry a complex protein cargo

In order to identify proteins that were specifically enriched in the PLY-released microvesicles and, therefore might play a role in plasmalemmal repair, we compared the protein composition of the microvesicles with that of the total cellular membrane preparations, which contained components originating from both the plasma membrane as well as from the intracellular membranes. The latter preparation was selected as a reference since microvesicles are expected to originate from plasmalemmal folds that are devoid of cytosolic components and also the intracellular membranes (e.g. lysosomes [26]) are expected to play a role in the process of plasmalemmal repair. Analysis of the total protein concentration revealed that 8% ± 4% SD (N = 6) of total membrane protein mass was emitted as microvesicular protein cargo at sub-lytic [PLY]. Western blot analyses of individual proteins demonstrated that 5% ± 5% SD (N = 4) of membrane-associated Hsp90 was expelled with microvesicles, which is comparable to the amount of total protein released with microvesicles and, thus suggests its random and equal distribution on the plasmalemma and on the released microvesicles (Supplementary Figure 8). However, 33% ± 22% SD (N = 6) of membrane-associated annexin A6 (~4-fold enrichment compared to the released total protein mass (~8%)) and 22% ± 20% SD (N = 5) of membrane-associated annexin A2 (~2-3-fold enrichment) were detected in the microvesicular fraction, which is indicative of their specific accumulation within microvesicles (Supplementary Figure 8).

Mass spectrometric analysis of the protein composition of PLY-released microvesicles and of purified total membranes (3 independent experiments) yielded 1073 proteins in the microvesicle fraction compared to 1036 in the total membrane isolate. This is a very sensitive method, therefore it is only to be expected that many of these proteins are contaminants. These could originate from the cytosol and the intracellular compartments of cells that were lysed by PLY or during experimental handling or might belong to the content of broken (and vesiculated) cellular protrusions depicted in Supplementary Figure 7. In total, 190 proteins were enriched in the microvesicle fraction compared to the fraction of total cellular

27

membranes in all 3 experiments (Supplementary File 2). We are aware that the total

membrane fraction or any other isolate are not a precise match for the microvesicles and

therefore do not consider enrichment *per se* as a well-defined indicator of a selective

presence of a particular protein within the microvesicle fraction. Hence we applied a more

stringent criterion of at least 4-fold enrichment in all 3 experiments, which yielded 38 proteins

(Table 2). Prominent members of these were annexins A6, A7 and A11 together with several

other Ca^{2+}-sensing proteins, actin-binding proteins, components of the ESCRT-I complex

and proteins that are involved in the intracellular vesicle trafficking (Table 2).

Table 2: Mass spectrometric analysis of isolated microvesicles. *Proteins with an at least four-fold increased PMSS index in microvesicles compared to total membrane isolates in all individual experiments are listed (HEK 293 cells; N = 3).*

Pneumolysin
Ca^{2+}-dependent or Ca^{2+}-regulated:
Annexin A6
Annexin A7
Annexin A11
Calcyclin-binding protein
Calpain-1 catalytic subunit
Nucleobindin-1
Peflin
Tumor protein D52
Actin-binding:
Calponin-3
Plastin-2
Plastin-3
Transgelin-2
Unconventional myosin-Ic
Vesicular trafficking/ESCRT-components:
ADP-ribosylation factor-like protein 1
Flotillin-2
GTP-binding protein SAR1a
Programmed cell death 6-interacting protein
Syntenin-1
Tumor susceptibility gene 101 protein
Unconventional myosin-Ic
Unconventional myosin-Id
Ubiquitin fusion degradation protein 1 homolog
Vacuolar protein sorting-associated protein 28 homolog
Heat shock protein-/chaperone-associated:
DnaJ homolog subfamily B member 1
DnaJ homolog subfamily A member 2
DnaJ homolog subfamily C member 7
Prefoldin subunit 5
Stress-induced-phosphoprotein 1
Enzymes:
Casein kinase II subunit alpha'
Malate dehydrogenase, mitochondrial

Peroxiredoxin-2
Pyruvate kinase isozymes M1/M2
Thioredoxin-dependent peroxide reductase, mitochondrial
Tetraspanin-/Immunoglobulin super family-associated:
CD9 antigen
Immunoglobulin superfamily member 8
Junctional adhesion molecule A
Prostaglandin F2 receptor negative regulator
RNA-associated:
Eukaryotic translation initiation factor 4 gamma 2
Eukaryotic translation initiation factor 5A-1
Far upstream element-binding protein 1
Far upstream element-binding protein 2
Others:
Integrin alpha-5 light chain
Monocarboxylate transporter 1
Suppressor of G2 allele of SKP1 homolog
Synapse-associated protein 1

4. Discussion

4.1. Repair of plasmalemmal toxin pores is critical for the cellular response to early pneumococcal invasion

Pneumolysin (PLY) is the most prevalent virulence factor of *Streptococcus pneumoniae*. Its assembly into large transmembrane pores leads to perforation of the plasmalemma of the host cells, which might result in immediate lysis. Our data suggest that during pneumococcal infection PLY is released in amounts that are sufficient to permeabilize host cells. In general, cells are capable of repairing the PLY-induced plasmalemmal lesions. Their ability to withstand low amounts of PLY is crucial for the course of infection since "non-lytic" [PLY] trigger the release of pro-inflammatory cytokines and the recruitment of immune cells [30-32]. Our data suggest that PLY-induced activation of cellular signaling can occur even without a specific receptor and it appears to be a result of successful repair of the PLY-perforated plasmalemma since the effective plasmalemmal repair in perforated cells is accompanied by transient elevation in $[Ca^{2+}]_i$ [9, 13, 18, 21, 33], which is a major second messenger. On the other hand, dysregulation of cellular homeostasis occurring as a result of transient, pore-induced entry of calcium ions might be responsible for the long-term damaging toxin action since high $[Ca^{2+}]_i$ is a potent activator of apoptosis.

4.2. Microvesicle release is the membrane repair strategy of choice

The fact that several, seemingly mutually excluding mechanisms have been advocated for plasmalemmal repair of toxin-perforated cells, rev. by [7, 25, 34, 35] points to its critical importance for cellular survival. It is likely that the repair strategy of choice depends as much on the nature and the extent of the damage, as on the metabolic status of damaged cells and even on their geometry [13].

In either case, toxin-perforation leads to Ca^{2+}-influx and subsequently to the mobilization of the Ca^{2+}-dependent plasma membrane repair machinery [25] which attempts to immediately neutralize the injury in order to prevent noxious Ca^{2+}-flooding and to restore plasma membrane integrity [9, 18, 21, 33]. We have shown that after perforation, Ca^{2+}-dependent members of the annexin protein family are recruited to the plasma membrane [9, 18, 21, 36] resealing the sites of excessive Ca^{2+}-influx and allowing the cell to quarantine the damaged membrane regions [13, 18, 21, 33]. The annexin-driven plugging of the initial toxin-induced plasmalemmal perforations is crucial: plasmalemmal repair is severely compromised in cells in which expression of either annexin A1 or annexin A6 was down-regulated [21, 33]. There is also sufficient evidence that the plasmalemmal repair mechanisms described here in molecular detail are not restricted to the toxin-induced perforations [37] and are also operative *in vivo* [25]. In particular annexin A1 has been implicated in epithelial repair of inflamed stomach and colon [38, 39], while annexin A5 is upregulated in neurons and glia in rats after experimental spinal cord trauma [40].

The plugged toxin pores are removed by shedding of the affected regions into the extracellular milieu in the form of microvesicles/ectosomes [13, 18, 21]. Ectosomal, microvesicular structures are credited with clinical importance since they do not only act as biomarkers but are also implicated in short and long distance intercellular communication [41-43]. An alternative route for the removal of toxin pores is represented by intracellular uptake, following pore-induced fusion of lysosomes with the damaged plasmalemma, as has previously been shown for the elimination of SLO pores [26].

30

Here we show that microvesicular release is associated with the formation of thin nanotubes that originate on the plasmalemma of cells treated with *S. pneumoniae* and that appear to break down by releasing microvesicular material into the extracellular milieu. Released microvesicles were relatively small (median = 163 nm) with more than 90% of them being smaller than 500 nm. Larger PLY-containing vesicles observed in this study or SLO-containing blebs that were reported earlier [28] might be a sub-product of nanotube-induced microvesicle shedding; otherwise they might originate from the heavily damaged cells [13]. It is conceivable that the release of microvesicles occurs spontaneously since nanotubes that sprout from toxin-attacked cells are so thin that they might break off passively, either by Brownian motion or by shear stress. Toxin-induced blebbing in chemically fixed cells [28] has previously been taken as evidence for spontaneous plasmalemmal resealing which is driven by rearrangement of the plasmalemmal lipid-bilayer. We have addressed the possibility of passive microvesicle shedding, exclusively driven by the physical action of the toxin on the membrane rather than by the active contribution of cellular proteins [28] but we were unable to affirm the presence of this particular mechanism.

On the other hand, active modes of microvesicle formation cannot be excluded. Annexins possess membrane fusogenic activity, and thus might be responsible for microvesicle release [25, 44], or else the shedding of toxin-perforated membrane sites is mediated by components of the ESCRT-III complex (Chmp4B, Vps4; [15]). A Ca^{2+}-dependent accumulation of components of the ESCRT-III complex has previously been shown to be followed by outward budding and scission of the damaged sites in plasmalemmal repair of laser- and toxin induced cellular injuries [15]. This study [15] did not find evidence for a contribution of annexin A1 in membrane repair, which might indicate that the injury model described by Jimenez et al. (2014) [15] did not induce sufficient Ca^{2+}-influx for the recruitment of annexin A1 to the perforated plasmalemmal sites (20 µM is required for annexin A1) [9]. However, the presence of more sensitive annexins such as A2, A6 or A11 was not investigated and thus cannot be excluded. Although we failed to observe an association of Chmp4B with the plasmalemma of PLY-perforated cells, we found that the

31

ESCRT-I components Tsg101 and Vps28 were highly enriched in the preparations of purified shed microvesicles.

4.3. PLY pores within released microvesicles structurally resemble those in artificial membranes

PLY prepore and pore structures in artificial liposomes are well characterized by cryo-electron microscopy [29]. In addition, the packing of monomers in the prepore complex has been described by crystallography [45]. The plasma membrane of living cells differs from artificial liposomes as regards lipid composition, the presence of an extracellular matrix, peripheral and integral membrane proteins and, importantly, by its ability to actively react to a toxin-attack. Yet, the diameters of toxin pores in sample preparations of PLY-containing microvesicles are only slightly different than the ones that have been described in artificial liposome membranes [29].

4.4. Microvesicles are selectively enriched in proteins instigating membrane repair and vesicular trafficking

The mass spectrometric analysis of the PLY-induced microvesicle isolate yields a complex protein cargo with annexins among the most prevalent proteins, further supporting their active role in plasmalemmal repair. We found that other Ca^{2+}-regulated proteins, such as peflin and the calpain 1 catalytic subunit are highly enriched in microvesicles. The enrichment in the microvesicular fraction of several actin-binding proteins (transgelin 2, myosin Ic) is in line with the contribution of the actin cortex in plasmalemmal resealing [13, 33, 34]. The apoptosis-linked gene 2 (ALG-2) and ALIX (ALG-2 interacting protein X) have been described to direct ESCRT-III proteins to the perforated sites in a Ca^{2+}-dependent manner [15]. It is interesting to note that ALG-2 has been reported to interact with N-terminal Pro-rich regions of annexin A7 and A11 [46, 47], suggestive of a potential link between the annexin family and the ESCRT complex. Interestingly, cryo-electron tomography showed that high density material was frequently locally concentrated within microvesicles under PLY

32

structures. In all likelihood, this material corresponds to the proteins detected by mass spectrometry. In particular, the accumulation of the annexins directly at the damaged sites of plasmalemma ([9, 21]; Figure 2) is well documented and the formation of two-dimensional annexin A5 arrays at the sites of plasmalemmal injury has been recently reported [37].

5. Conclusions

S. pneumoniae releases sufficient PLY for toxin-induced plasmalemmal perforation in host cells, however, at least in the initial stages of infection, repair mechanisms are highly effective. Therefore, an immediate and straightforward cell lysis, which is frequently reported in the literature as a result of treatment with purified and artificially concentrated toxins, appears to be an unlikely event *in vivo*. Our data suggest that it is rather the dysregulation of cellular homeostasis occurring as a result of transient, pore-induced entry of second-messenger calcium ions that should be held responsible for the damaging toxin action. We present evidence that active microvesicle shedding is the predominant mechanism of toxin removal and that PLY is not internalized or shed in a passive process. Detailing the structure of PLY-oligomers on biological membranes, we demonstrate that prepores and functional pores are likewise removed. The protein composition of the toxin-induced vesicles is suggestive of a Ca^{2+}-triggered mechanisms involving the annexin protein family and members of the ESCRT complex.

Author contributions

H. W. and J. R. performed experiments and wrote the paper. R. S., R. K., P. D., V. S. B. and E. B. B. performed experiments. T.J.M. provided the PLY-mutant ΔA146R147-GFP and L. J. H. provided supernatants of the clinical pneumococcal strains. B. Z. edited the paper and supervised electron microscopy. A.D. and E.B.B. designed the study and wrote the paper. All authors analyzed and discussed the results and commented on the manuscript.

Competing interests

No competing interests.

References

[1] K.L. O'Brien, L.J. Wolfson, J.P. Watt, E. Henkle, M. Deloria-Knoll, N. McCall, E. Lee, K. Mulholland, O.S. Levine, T. Cherian, H.P.G.B. Dis, Burden of disease caused by Streptococcus pneumoniae in children younger than 5 years: global estimates, Lancet, 374 (2009) 893-902.

[2] T.J. Mitchell, C.E. Dalziel, The biology of pneumolysin, Subcell Biochem, 80 (2014) 145-160.

[3] R. Cockeran, R. Anderson, C. Feldman, The role of pneumolysin in the pathogenesis of Streptococcus pneumoniae infection, Curr Opin Infect Dis, 15 (2002) 235-239.

[4] C.J. Rosado, S. Kondos, T.E. Bull, M.J. Kuiper, R.H.P. Law, A.M. Buckle, I. Voskoboinik, P.I. Bird, J.A. Trapani, J.C. Whisstock, M.A. Dunstone, The MACPF/CDC family of pore-forming toxins, Cellular Microbiology, 10 (2008) 1765-1774.

[5] M.R. Gonzalez, M. Bischofberger, L. Pernot, F.G. van der Goot, B. Freche, Bacterial pore-forming toxins: the (w)hole story?, Cell Mol Life Sci, 65 (2008) 493-507.

[6] R.K. Tweten, Cholesterol-dependent cytolysins, a family of versatile pore-forming toxins, Infect Immun, 73 (2005) 6199-6209.

[7] E.B. Babiychuk, A. Draeger, Defying death: Cellular survival strategies following plasmalemmal injury by bacterial toxins, Semin Cell Dev Biol, 45 (2015) 39-47.

[8] T.C. Barnett, J.N. Cole, T. Rivera-Hernandez, A. Henningham, J.C. Paton, V. Nizet, M.J. Walker, Streptococcal toxins: role in pathogenesis and disease, Cell Microbiol, 17 (2015) 1721-1741.

[9] H. Wolfmeier, R. Schoenauer, A.P. Atanassoff, D.R. Neill, A. Kadioglu, A. Draeger, E.B. Babiychuk, Ca-dependent repair of pneumolysin pores: A new paradigm for host cellular defense against bacterial pore-forming toxins, Biochim Biophys Acta, (2014).

[10] N.W. Andrews, F. Perez, The plasma membrane repair shop: Fixing the damage, Semin Cell Dev Biol, 45 (2015) 1.

[11] A.K. McNeil, U. Rescher, V. Gerke, P.L. McNeil, Requirement for annexin A1 in plasma membrane repair, J Biol Chem, 281 (2006) 35202-35207.

[12] T. Castro-Gomes, M. Corrotte, C. Tam, N.W. Andrews, Plasma Membrane Repair Is Regulated Extracellularly by Proteases Released from Lysosomes, Plos One, 11 (2016).

[13] A.P. Atanassoff, H. Wolfmeier, R. Schoenauer, A. Hostettler, A. Ring, A. Draeger, E.B. Babiychuk, Microvesicle shedding and lysosomal repair fulfill divergent cellular needs during the repair of streptolysin O-induced plasmalemmal damage, Plos One, 9 (2014) e89743.

[14] K. Monastyrskaya, E.B. Babiychuk, A. Hostettler, U. Rescher, A. Draeger, Annexins as intracellular calcium sensors, Cell Calcium, 41 (2007) 207-219.

[15] A.J. Jimenez, P. Maiuri, J. Lafaurie-Janvore, S. Divoux, M. Piel, F. Perez, ESCRT Machinery Is Required for Plasma Membrane Repair, Science, 343 (2014) 986-+.

[16] A.M. Berry, A.D. Ogunniyi, D.C. Miller, J.C. Paton, Comparative virulence of Streptococcus pneumoniae strains with insertion-duplication, point, and deletion mutations in the pneumolysin gene, Infect Immun, 67 (1999) 981-985.

[17] L.A.S. Kirkham, A.R. Kerr, G.R. Douce, G.K. Paterson, D.A. Dilts, D.F. Liu, T.J. Mitchell, Construction and immunological characterization of a novel nontoxic protective pneumolysin mutant for use in future pneumococcal vaccines, Infection and Immunity, 74 (2006) 586-593.

[18] E.B. Babiychuk, K. Monastyrskaya, S. Potez, A. Draeger, Intracellular Ca2+ operates a switch between repair and lysis of streptolysin O-perforated cells, Cell Death and Differentiation, 16 (2009) 1126-1134.

[19] J. Colinge, D. Chiappe, S. Lagache, M. Moniatte, L. Bougueleret, Differential proteomics via probabilistic peptide identification scores, Anal Chem, 77 (2005) 596-606.

[20] J. Schindelin, I. Arganda-Carreras, E. Frise, V. Kaynig, M. Longair, T. Pietzsch, S. Preibisch, C. Rueden, S. Saalfeld, B. Schmid, J.Y. Tinevez, D.J. White, V. Hartenstein, K. Eliceiri, P. Tomancak, A. Cardona, Fiji: an open-source platform for biological-image analysis, Nat Methods, 9 (2012) 676-682.

[21] S. Potez, M. Luginbul, K. Monastyrskaya, A. Hostettler, A. Draeger, E.B. Babiychuk, Tailored Protection against Plasmalemmal Injury by Annexins with Different Ca2+ Sensitivities, Journal of Biological Chemistry, 286 (2011) 17982-17991.

[22] J.R. Kremer, D.N. Mastronarde, J.R. McIntosh, Computer visualization of three-dimensional image data using IMOD, Journal of Structural Biology, 116 (1996) 71-76.

[23] K.A. Benton, J.C. Paton, D.E. Briles, Differences in virulence for mice among Streptococcus pneumoniae strains of capsular types 2, 3, 4, 5, and 6 are not attributable to differences in pneumolysin production, Infection and Immunity, 65 (1997) 1237-1244.

[24] J.R. Canvin, A.P. Marvin, M. Sivakumaran, J.C. Paton, G.J. Boulnois, P.W. Andrew, T.J. Mitchell, The Role of Pneumolysin and Autolysin in the Pathology of Pneumonia and Septicemia in Mice Infected with a Type-2 Pneumococcus, Journal of Infectious Diseases, 172 (1995) 119-123.

[25] A. Draeger, K. Monastyrskaya, E.B. Babiychuk, Plasma membrane repair and cellular damage control: The annexin survival kit, Biochemical Pharmacology, 81 (2011) 703-712.

[26] V. Idone, C. Tam, J.W. Goss, D. Toomre, M. Pypaert, N.W. Andrews, Repair of injured plasma membrane by rapid Ca2+-dependent endocytosis, Journal of Cell Biology, 180 (2008) 905-914.

[27] V. Kralj-Iglic, Stability of membranous nanostructures: a possible key mechanism in cancer progression, Int J Nanomedicine, 7 (2012) 3579-3596.

[28] P.A. Keyel, L. Loultcheva, R. Roth, R.D. Salter, S.C. Watkins, W.M. Yokoyama, J.E. Heuser, Streptolysin O clearance through sequestration into blebs that bud passively from the plasma membrane, Journal of Cell Science, 124 (2011) 2414-2423.

[29] S.J. Tilley, E.V. Orlova, R.J. Gilbert, P.W. Andrew, H.R. Saibil, Structural basis of pore formation by the bacterial toxin pneumolysin, Cell, 121 (2005) 247-256.

[30] S. Shoma, K. Tsuchiya, I. Kawamura, T. Nomura, H. Hara, R. Uchiyama, S. Daim, M. Mitsuyama, Critical involvement of pneumolysin in production of interleukin-1alpha and caspase-1-dependent cytokines in infection with Streptococcus pneumoniae in vitro: a novel function of pneumolysin in caspase-1 activation, Infect Immun, 76 (2008) 1547-1557.

[31] R. Cockeran, C. Durandt, C. Feldman, T.J. Mitchell, R. Anderson, Pneumolysin activates the synthesis and release of interleukin-8 by human neutrophils in vitro, J Infect Dis, 186 (2002) 562-565.

[32] S. Houldsworth, P.W. Andrew, T.J. Mitchell, Pneumolysin stimulates production of tumor necrosis factor alpha and interleukin-1 beta by human mononuclear phagocytes, Infect Immun, 62 (1994) 1501-1503.

[33] E.B. Babiychuk, K. Monastyrskaya, S. Potez, A. Draeger, Blebbing confers resistance against cell lysis, Cell Death Differ, 18 (2011) 80-89.

[34] P.L. McNeil, T. Kirchhausen, An emergency response team for membrane repair, Nat Rev Mol Cell Biol, 6 (2005) 499-505.

[35] V. Idone, C. Tam, N.W. Andrews, Two-way traffic on the road to plasma membrane repair, Trends Cell Biol, 18 (2008) 552-559.

[36] R. Schoenauer, A.P. Atanassoff, H. Wolfmeier, P. Pelegrin, E.B. Babiychuk, A. Draeger, P2X7 receptors mediate resistance to toxin-induced cell lysis, Biochim Biophys Acta, 1843 (2014) 915-922.

[37] R. Carmeille, F. Bouvet, S. Tan, C. Croissant, C. Gounou, K. Mamchaoui, V. Mouly, A.R. Brisson, A. Bouter, Membrane repair of human skeletal muscle cells requires Annexin-A5, Biochim Biophys Acta, 1863 (2016) 2267-2279.

[38] N. Vergnolle, P. Pages, R. Guimbaud, S. Chaussade, L. Bueno, J. Escourrou, C. Comera, Annexin 1 is secreted in situ during ulcerative colitis in humans, Inflamm Bowel Dis, 10 (2004) 584-592.

[39] G.R. Martin, M. Perretti, R.J. Flower, J.L. Wallace, Annexin-1 modulates repair of gastric mucosal injury, Am J Physiol Gastrointest Liver Physiol, 294 (2008) G764-769.

[40] N. Liu, S. Han, P.H. Lu, X.M. Xu, Upregulation of annexins I, II, and V after traumatic spinal cord injury in adult rats, J Neurosci Res, 77 (2004) 391-401.

[41] E. Cocucci, J. Meldolesi, Ectosomes and exosomes: shedding the confusion between extracellular vesicles, Trends in Cell Biology, 25 (2015) 364-372.

[42] M. Mittelbrunn, F. Sanchez-Madrid, Intercellular communication: diverse structures for exchange of genetic information, Nat Rev Mol Cell Biol, 13 (2012) 328-335.

[43] K. McCoy-Simandle, S.J. Hanna, D. Cox, Exosomes and nanotubes: Control of immune cell communication, Int J Biochem Cell Biol, 71 (2016) 44-54.

[44] V. Gerke, C.E. Creutz, S.E. Moss, Annexins: linking Ca2+ signalling to membrane dynamics, Nat Rev Mol Cell Biol, 6 (2005) 449-461.

[45] J.E. Marshall, B.H.A. Faraj, A.R. Gingras, R. Lonnen, M.A. Sheikh, M. El-Mezgueldi, P.C.E. Moody, P.W. Andrew, R. Wallis, The Crystal Structure of Pneumolysin at 2.0 angstrom Resolution Reveals the Molecular Packing of the Pre-pore Complex, Scientific Reports, 5 (2015).

[46] H. Satoh, Y. Nakano, H. Shibata, M. Maki, The penta-EF-hand domain of ALG-2 interacts with amino-terminal domains of both annexin VII and annexin XI in a Ca2+-dependent manner, Biochim Biophys Acta, 1600 (2002) 61-67.

[47] H. Satoh, Y. Nakano, H. Shibata, M. Maki, The penta-EF-hand domain of ALG-2 interacts with amino-terminal domains of both annexin VII and annexin XI in a Ca2+-dependent manner, Bba-Proteins Proteom, 1600 (2002) 61-67.

Highlights

S. pneumoniae releases sufficient PLY to perforate host cells.

PLY-induced plasmalemmal perforations are efficiently repaired.

Microvesicle shedding is the predominant mechanism of PLY-pore elimination.

PLY prepores are likewise removed.

Shed microvesicles are enriched in annexins and ESCRT proteins.